Molecular Crystals
Publication details, including instructions for authors and subscription information:
http://www.tandfonline.com/loi/gmcl15

The Paracrystal as a Model for Liquid Crystals

R. Hosemann [a], K. Lemm [a] & W. Wilke [a]
[a] Fritz-Haber-Institut der Max-Planck-Gesellschaft, Berlin, Dahlem

Version of record first published: 21 Mar 2007.

To cite this article: R. Hosemann , K. Lemm & W. Wilke (1967): The Paracrystal as a Model for Liquid Crystals, Molecular Crystals, 2:4, 333-362

To link to this article: http://dx.doi.org/10.1080/15421406708083425

Molecular Crystals. 1967. Vol. 1, pp. 333–362

Printed in Great Britain

The Paracrystal as a Model for Liquid Crystals*

R. HOSEMANN, K. LEMM and W. WILKE
Fritz-Haber-Institut der Max-Planck-Gesellschaft, Berlin-Dahlem

Received December 6, 1965, *Revised June* 15, 1966

Abstract—It is emphasized, that the loss of long range order does not necessarily destroy three-dimensional lattices. Nematic or smectic mesophases as well as special types of liquid crystals, many crystalline or amorphous high polymers, crystals near the melting point, molten substances and mixed crystals are examples in nature. The theory of paracrystals describes such lattices quantitatively in a most convenient mathematical way. A very short survey of the main formulas is given, which are needed for a practical application of the theory to X-ray, electron and neutron diffraction problems. The derivations are given in standard texts.[1,2] This publication is confined to the discussion of the integral widths of the reflections.

Two reasons for line broadening are discussed: paracrystalline distortions and particle size effects. It will be shown how one can separate these two effects and also the effect of thermal oscillations. These results are applied in a separate section to the analysis of paracrystalline mosaic blocks in single polyethylene crystals and paracrystalline ultrafibrils in stretched polyethylene. The mosaic blocks have sizes of about 300 Å and g-values = 2%, the ultrafibrils diameters of 100 Å and $g = 3\%$. 2° C below and some degrees above the melting point lead also consists of such micro-paracrystallites. Their mean size 23° C above the melting point is 30 Å, $g = 11.5\%$, 223° C above the melting point 10 Å, $g = 12.5\%$. 2° C below the melting point g drops down to 4%. At the melting point a network of paracrystalline grain-boundaries arises suddenly, whilst the thermal and paracrystalline distortions within the paracrystals increase more or less continuously with rising temperature. Inside the paracrystals subgroups of atoms exist with a smaller amount of paracrystalline distortion. All liquid metals investigated by us, at least up to 100° C above the melting point, can be explained quantitatively by aggregates of clusters of atoms in paracrystalline distorted hexagonal close packing. Mixed crystals of α-Fe with 15 atom % Al have g-values of 1%, whilst rigid atoms should have g-values about twice as large. This discrepancy can be explained by the deformability of the electron clouds. A Laves phase (Fe_2Zr) has g-values up to 0.7%, reduced Fe, Al-spinels (3 atom % Al) have g-values near 1%. The para-

* Based on a lecture presented at the International Liquid Crystal Conference, Kent State University, Kent, Ohio, August 16–20, 1965.

crystalline distortions show characteristic anisotropies, which give some information about the arrangement of the foreign atoms or subgroups in the lattice.

I. Introduction

If in an α-Fe lattice some of its atoms are replaced by larger Al-atoms, lattice distortions occur. If the atoms behave like incompressible liquid droplets, this distortion decreases as $1/r^2$ and the long range order is preserved.[18] In reality the electron clouds have a shear modulus, which is not negligibly small. Hence the long range order must be destroyed. Similar problems arise, if we discuss a lattice with thermal vibrations. Only in a first approximation do the electron clouds oscillate like rigid entities. If the temperature is not small enough compared with the characteristic temperature, correlations with the adjacent atoms occur and the electron clouds are deformed. As a consequence, the thermoelastic waves are damped and hence different lattice cells have different oscillation volumes. Again the long range order breaks down.[11] In many high polymers at least one direction is characterized by van der Waals' forces with a relatively low characteristic temperature. In addition, paracrystalline distortions are produced by the conformation of the complicated molecules. Last but not least, mesophases play an important role in the glassy state. They can be described as special degenerate cases of paracrystals. The same is true for the conventional theories of liquids and crystals, which are special structures within the more general concept of paracrystals (cf. the following table):

Principal States of Aggregation

	Crystal	Paracrystal	Liquid	Amorphous and gaseous
Long range order	+	−	−	−
Lattices	+	+	−	−
Identical *a priori* probability	−	+	+	−
Spherically symmetric correlation function $Q(r)$	−	−	+	+

In the presence of thermal vibrations, the atoms of a crystal do not have the same *a priori* pair correlation function. As a direct consequence of the long range order, an atom A oscillating in direction 1 has a different distance distribution, with respect to the rest of the lattice, than an atom B oscillating in direction 2. In the concept of paracrystals the classic assumption of Debye and Zernike-Ornstein is preserved, namely that each atom has the same *a priori* distance distribution with respect to all the other atoms. The difference from the Debye-concept lies in the fact that, in the paracrystal theory, the idea of three-dimensional lattices remains preserved. As a next step thermal oscillations of the atoms around the lattice points of the paracrystal can be introduced.

Starting from this most general assumption a theory of structure and its Fourier transform, which by means of the Ewald construction gives the diffraction patterns, can be developed with a minimum of correlation functions. This is called the "ideal paracrystal". It is a first approximation, good enough to describe the following structures. In a real paracrystal a certain number of correlation correction terms is introduced. (For details see reference 1)

II. Theoretical Background

The scattered intensity from an object, composed of atomic groups with structure factor $F(\mathbf{b})$ and having an atomic density distribution $\rho_a(\mathbf{x})$, is given by

$$I(\mathbf{b}) = |F(\mathbf{b})|^2 . \mathcal{F} Q_a(\mathbf{x}) \tag{1}$$

$\mathcal{F}$ is the Fourier-transform operator

$$\mathcal{F} = \int dv_x \exp(-2\pi i \mathbf{b}\mathbf{x}) \tag{2}$$

$Q_a(\mathbf{x})$ the folding square of $\rho_a(\mathbf{x})$,

$$Q_a(\mathbf{x}) = \int \rho_a(\mathbf{y})\,\rho_a(\mathbf{x}+\mathbf{y})\,dv_y = \rho_a(\mathbf{x}) \widetilde{\rho_a}(-\mathbf{x}) = \overset{2}{\widetilde{\rho_a}}(\mathbf{x}) \tag{3}$$

and

$$\mathbf{b} = \frac{\mathbf{s}-\mathbf{s}_0}{\lambda} \qquad |\mathbf{b}| = \frac{2\sin\vartheta}{\lambda} \tag{4}$$

$\mathbf{s}$, $\mathbf{s}_0$ = unit vectors in the directions of the primary and diffracted beam

2ϑ = diffraction angle

λ = wave length of the X-rays.

If $\rho_{a\infty}(\mathbf{x})$ is the atomic density distribution function in an infinitely extended structure, the density distribution of a finite object is given by

$$\rho_a(\mathbf{x}) = \rho_{a\infty}(\mathbf{x})\, s(\mathbf{x}) \tag{5}$$

$s(\mathbf{x})$ is the shape function or form factor of the object with volume V and has the properties

$s(\mathbf{x})$ = 1 inside the external surface of the finite object

= 0 outside the finite object

$$\int s(\mathbf{x})\, dv_x = \int s^2(\mathbf{x})\, dv_x = V \tag{6}$$

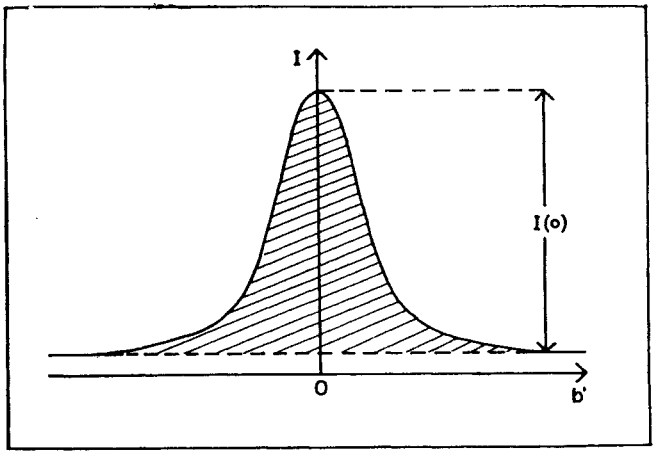

Figure 1. Integral width of a reflection. $\delta\beta$ is given by the quotient of the dashed area and $I(0)$ (cf. Reference 1, p. 322).

For the diffracted intensity from a finite object one then obtains from Eqs. (1) and (5)

$$I(\mathbf{b}) = \frac{|F(\mathbf{b})|^2}{\bar{v}_m} Z(\mathbf{b}) \widehat{|S(\mathbf{b})|^2} \tag{7}$$

$$Z(\mathbf{b}) = \mathcal{F} z(x) = \frac{v_m}{V} \mathcal{F} Q_a(x) \tag{7a}$$

$S(\mathbf{b}) = \mathcal{F} s(\mathbf{x})$ is the shape factor and $Z(\mathbf{b})$ the lattice factor, the Fourier-transform of the distance statistics function $z(\mathbf{x})$. $\bar{v}_m$ denotes

the average volume occupied by an atomic group. The introduction of thermal motions of the atoms gives no contribution to the integral line width, the only interesting quantity in our discussion. So the contributions to the measured integral width (cf. Fig. 1)

$$\delta\beta = \frac{\int_{\text{refl.}} I(\mathbf{b}')\,db'}{I(0)} \tag{8}$$

come from the widths of $Z(\mathbf{b})$ and $|S(b)|^2$. $|S(b)|^2$ gives an integral width (for powder diagrams)[3]

$$\delta\beta(|S_{23}|^2) = \frac{1}{\bar{L}_{23}} \tag{9}$$

which is determined by the average length of crystallites perpendicular to the diffracting lattice planes. To calculate the integral widths of the humps of the lattice factor $Z(\mathbf{b})$ we must make an assumption about the distribution of the atoms in the substance. For an ideal paracrystalline lattice [1] the distance statistics function is given by

$$z(\mathbf{x}) = \sum_{p_1}\sum_{p_2}\sum_{p_3} H^{(\mathbf{x})}_{p_1p_2p_3} = \sum_{p_1=-\infty}^{+\infty} H^{(\mathbf{x})}_{p_100} \sum_{p_2=-\infty}^{+\infty} H^{(\mathbf{x})}_{0p_20} \sum_{p_3=-\infty}^{+\infty} H^{(\mathbf{x})}_{00p_3} \tag{10}$$

with

$$H^{(\mathbf{x})}_{p_1p_2p_3} = P(\mathbf{x}-0)\overbrace{H_1(\mathbf{x})\ldots H_1(\mathbf{x})}^{|p_1|\text{-times}}\overbrace{H_2(\mathbf{x})\ldots H_2(\mathbf{x})}^{|p_2|\text{-times}}\overbrace{H_3(\mathbf{x})\ldots H_3(\mathbf{x})}^{|p_3|\text{-times}} \tag{11}$$

the distribution function around the vector

$$\mathbf{x}_{p_1p_2p_3} = p_1\bar{\mathbf{a}}_1 + p_2\bar{\mathbf{a}}_2 + p_3\bar{\mathbf{a}}_3 \tag{12}$$

$H_k(\mathbf{x})$ is the coordination statistic for the vector $\mathbf{a}_k$. The Fourier transform of $z(\mathbf{x})$, called paracrystalline lattice factor $Z(\mathbf{b})$, is given by

$$Z(\mathbf{b}) = \prod_{k=1}^{3} K_k(\mathbf{b});\ K_k(\mathbf{b}) = Re\frac{1+F_k(\mathbf{b})}{1-F_k(\mathbf{b})};\ F_k(\mathbf{b}) = \mathscr{F}H_k(\mathbf{x}) \tag{10a}$$

One of the K-factors is drawn schematically in Fig. 2. The width of the hump $H^{(\mathbf{x})}_{p_1p_2p_3}$ of $z(\mathbf{x})$ in the direction i is given for Gaussian like $H_k(\mathbf{x})$ by

$$\Delta^2_{p_1p_2p_3}x_i = \sum_{k=1}^{3} p_k\,\Delta^2_k x_i \tag{13}$$

where $\Delta_k^2 x_i$ is the standard deviation of $H_k(\mathbf{x})$ in direction i. The integral width of $Z(\mathbf{b})$ for a reflection of order h is then given by (for a Debye–Scherrer line)[4, 5] (cf. Figs. 2 and 3)

$$\delta\beta(Z) = \frac{\pi^2}{|\bar{\mathbf{a}}_k|} g_{kk}^2 h_k^2 \tag{14}$$

g_{ik} is the relative fluctuation of the vector $\mathbf{a}_k$ in direction i

$$g_{ik}^2 = \frac{\Delta_k^2 x_i}{|\bar{\mathbf{a}}_k|^2} \tag{15}$$

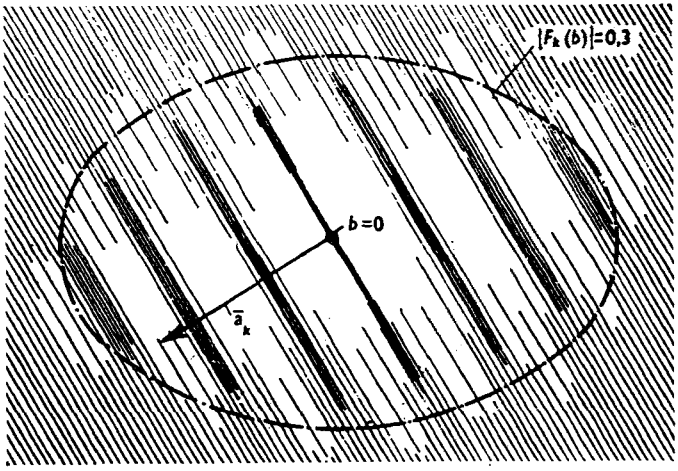

Figure 2. Schematic diagram of a K-factor on a plane passing through $\mathbf{b}=0$ and parallel to $\bar{a}_k$. Outside the ellipsoid this K-factor gives no contribution to the interferences.

The measurable integral width $\delta\beta$ after Eq. (7) is obtained from a function, which is the folding of $Z(\mathbf{b})$ and $|S(\mathbf{b})|^2$ and therefore dependent on the form of the functions $Z(\mathbf{b})$ and $|S(\mathbf{b})|^2$. If both functions are Gaussian-like (prop. $\exp(-\sigma b^2)$) one knows, that the integral widths add quadratically (cf. Eq. (13)). This is a good approximation and from Eqs. (7), (8) and (14) (neglecting indices for simplicity) one obtains

$$\delta\beta^2 = \delta\beta^2(|S_{23}^2|) + \delta\beta^2(Z) = \frac{1}{\bar{L}^2} + \frac{1}{|\bar{\mathbf{a}}|^2}(\pi g h)^4 \tag{16}$$

or

$$\delta\beta^2_{(\mathrm{h})} = (\delta\beta \,.\, |\bar{\mathbf{a}}|)^2 = \frac{1}{\bar{N}^2} + (\pi g h)^4 \tag{17}$$

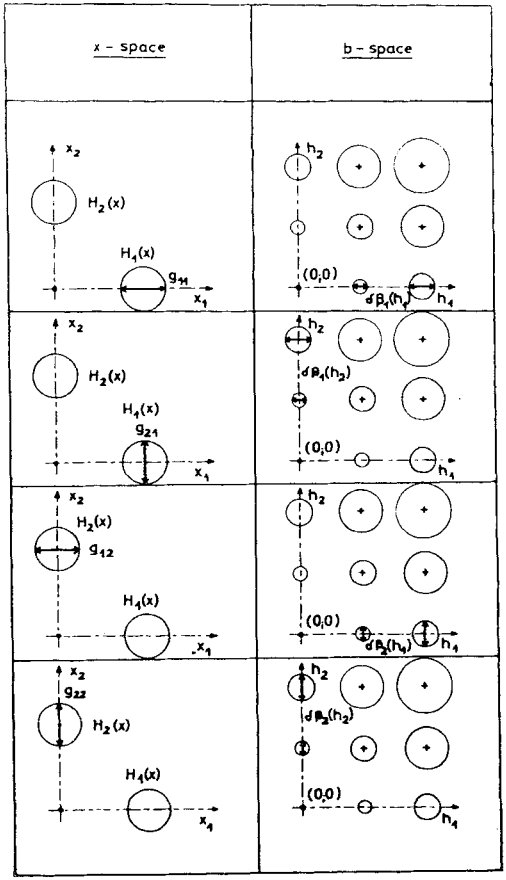

Figure 3. The relative statistical fluctuations g_{ik} of the coordination statistics $H_k(\mathbf{x})$ and the corresponding widths $\delta\beta_k(h_i)$ for a two-dimensional model (after Bonart[9]).

III. Applications

1. Polyethylene Single Crystals

As a first application we will give the measurement of the integral width of the reflections (110), (220) and (330) from polyethylene

crystals. These crystals were grown from a 0.05% solution of linear polyethylene Hostalen G (sample 1) and Lupolen 6011 H (sample 2) in Xylol. Fig. 4a shows a $\delta\beta'^2$-h^4 plot. If paracrystalline distortions are present, we should get a straight line in this plot as is indeed

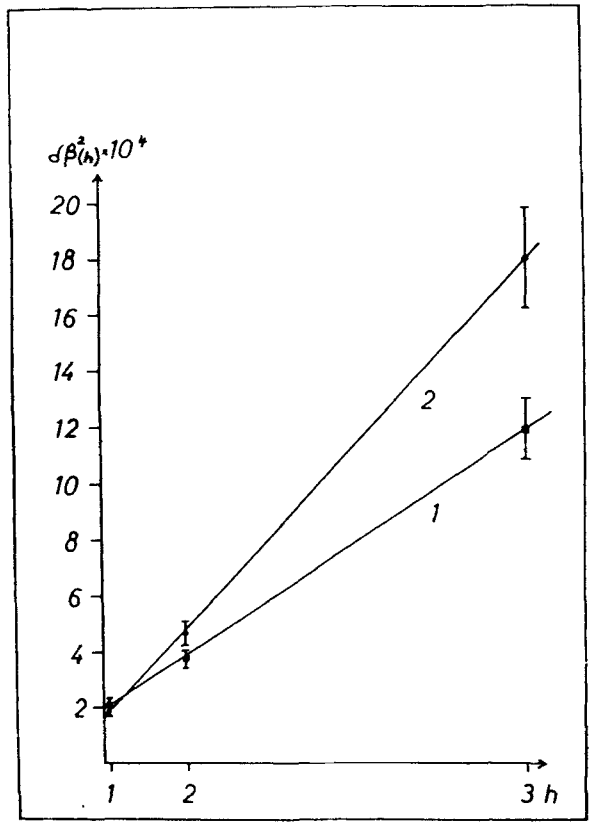

Figure 4a. $\delta\beta^2(h)$-h^4-diagram of the integral widths for the reflections (110), (220) and (330) from polyethylene single crystals (samples 1 and 2).

the case. Fig. 4b shows a $\delta\beta'^2$-h^2-diagram. If the line broadening arises from lattice strains, one would obtain a straight line in this plot. One can see that this is not possible in the case of polyethylene. In this manner it is possible to distinguish between line broadening caused by paracrystalline distortions and by lattice strains (cf. III, 4).

From the slope of the lines in Fig. 4a one calculates

$$g_1 = (1.88 \pm 0.07)\% \qquad g_2 = (2.14 \pm 0.06)\%$$

for the g-values of the two probes. They give the relative distance fluctuations of the (110)-planes. The average dimension of the

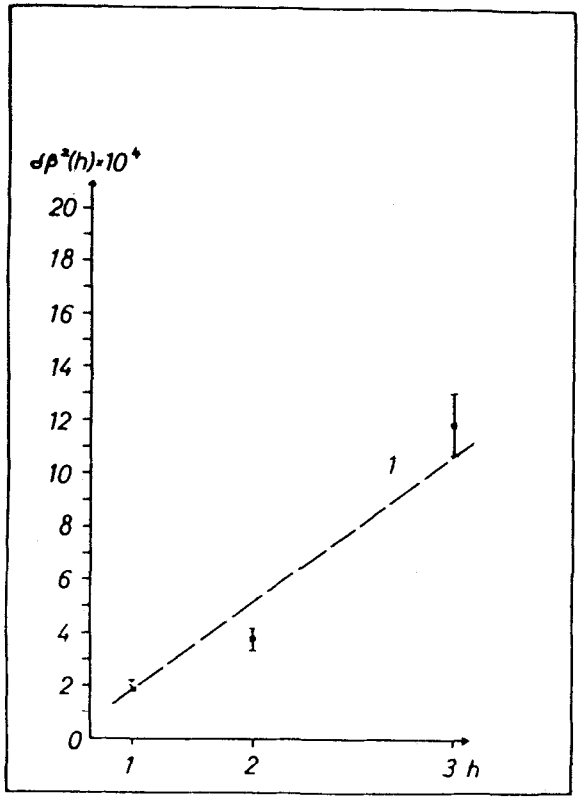

Figure 4b. $\delta\beta^2(h)$-h^2-diagram of the same measured integral widths (sample 1) as in Figure 4a. It is not possible to fit the points with a straight line.

coherently scattering regions perpendicular to the (110)-planes follows from the intersection with the ordinate ($h = 0$), and is given by

$$\bar{L}_1 = (299 \pm 20)\ \text{Å} \text{ and } \bar{L}_2 = (332 \pm 15)\ \text{Å}$$

Thus, this so-called single crystal has a mosaic structure with mosaic diameters of the order of 300 Å and paracrystalline distortions with $g \sim 2\%$. In another paper[6] we have proved that this is no contradiction to the observed Moiré patterns (cf. Fig. 5), which are extended about a few microns, if one assumes that the boundaries between adjacent mosaic blocks are twist boundaries.[7] The mosaic blocks are twisted about an axis lying perpendicular to the polyethylene chains, as shown in Fig. 6. The twist angle ϕ is of the

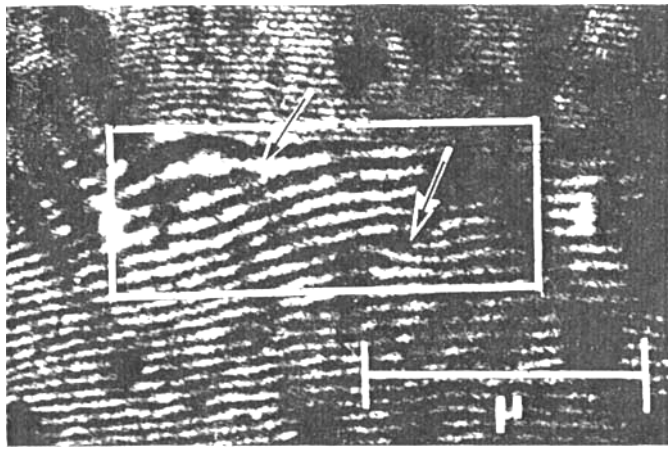

Figure 5. Moiré pattern (after Holland[10]) from a bilayered polyethylene single crystal. (Reflection at (200)). Two edge dislocations are marked by arrows.

order of 0.6°–11°. In this case the different mosaic blocks scatter the X-rays coherently and the Moiré-lines are on the average straight lines with a tumbling character as in Fig. 5, because the deviation from the straight line is proportional to ϕ^2.

2. Hot Stretched Polyethylene

A more complicated situation arises in hot stretched linear polyethylene (stretch ratio 60:1; stretched to 6:1 at 70° C and then at 120° C to 60:1). The reflections (110), (220) and (330) now have a profile, which is given by the sum of two Gaussian-like

functions. The analysis of the integral widths of this two terms (cf. Fig. 7), together with the analysis of the low angle scattering, leads to the conclusion[8] that this material consists of ultrafibrils with diameters of approximately 90 Å and paracrystalline distortions with $g \sim 3\%$. Four to nine of these ultrafibrils build a paracrystalline macrolattice. If the boundary between the ultrafibrils

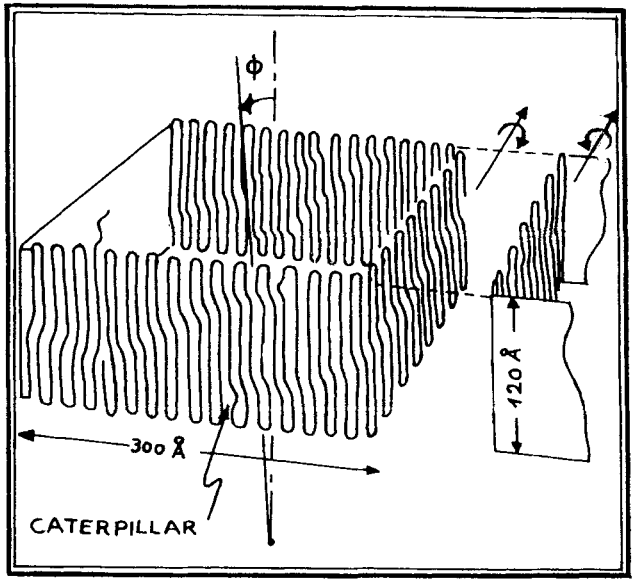

Figure 6. Model of a paracrystalline mosaic block in polyethylene single crystals with twist boundaries.

in these bundles consists of only one molecular layer, the relative statistical fluctuation within this layer is 42%, a very high value. Figure 8 shows a schematic picture of the cross-section through such a bundle of four ultrafibrils. One can see the less-distorted regions, separated by the highly distorted boundaries. It seems to us that this structure is a very good two dimensional model of a liquid.

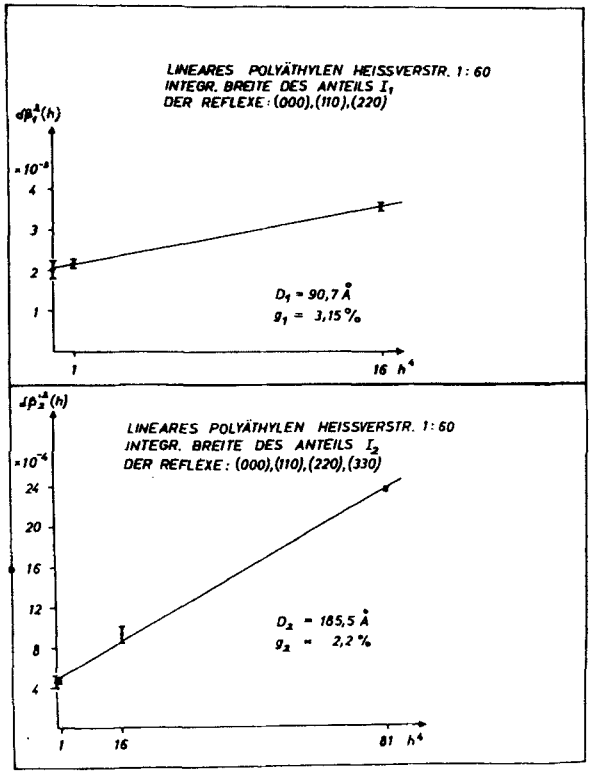

Figure 7. $\delta\beta^2(h)$-h^4-diagrams of the integral widths of the reflections (000) (low angle scattering) and (110), (220) and (330) for the two terms of the line profile. Hot stretched linear polyethylene, stretch ratio 1:60.

3. Monatomic Liquids near the Melting Point

In this section we will demonstrate that the X-ray and neutron diffraction of monatomic liquids near the melting point can be interpreted as being produced by a polyparacrystalline material. At this moment we cannot prove that the calculations give the unique solution. But this solution is a possible one and from the mathematical point of view the most elegant one. Moreover it has a high physical significance and fits well with the behaviour of matter below the melting point and with thermodynamical calcula-

tions of a liquid.[19] These micro-paracrystals exist only as a time average and may have a very short lifetime. The intensity function I of a liquid is in most cases a spherical symmetric function in

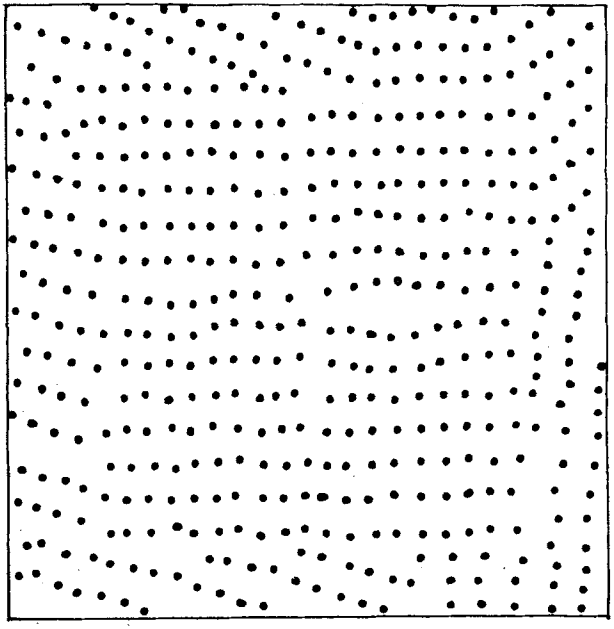

Figure 8. Model of a cross section of the fibrous structure in hot stretched polyethylene. Four paracrystalline distorted ultrafibrils build a bundle with high distorted boundaries.

Fourier space. Hence the Fourier-inverstransform, the Q-function defined by Eq. (3), is given by

$$Q(r) = \frac{2}{r}\int_0^\infty uI(u)\sin(2\pi ur)\,du \qquad u = |\mathbf{b}| \tag{18}$$

For monatomic liquids one starts with

$$i(u) = \frac{I - Nf^2}{Nf^2} \tag{19}$$

where N is the number of atoms and f^2 their scattering factor. Multiplying its Fourier-inverstransform by $4\pi r^2$ one obtains the so-called radial density distribution of the atoms:

$$4\pi r^2(z-\rho_0) = 8\pi r \int_0^\infty ui(u)\sin 2\pi ur\,du \tag{20}$$

where z is a convolution square (pair correlation function) of the centres of the atoms, defined by Eq. (7a). In the conventional theories it is called the density distribution $\rho(r)$ resp. $g(r)$. ρ_0 is the macroscopic density of the atoms in the liquid and, hence, gives the averaged number of atoms per Å^3.

The assumption used in our calculations[11] is, that $z(\mathbf{x})$ is given by a convolution polynom Eq. (10). In other words: The liquid can be described approximately as a single paracrystal. In reality this is certainly not the case. But our analysis will show that the coordination statistics $H_k(\mathbf{x})$ consist of two different kinds of distances: One kind of smaller values corresponding to neighboured atoms arranged in a crystalline-like manner, the other one defines larger distances, which correspond to neighboured atoms lying within grain boundaries, etc. In our calculation it is assumed that these larger distances are randomly distributed in the paracrystalline lattice. But it can be shown easily that the Q-function of a liquid remains nearly unchanged, if the smaller distances cluster in certain regions whilst the larger distances are concentrated on the boundaries of these clusters.

In other words: The following analysis on the basis of a single paracrystal with an inhomogeneous distance statistic (two kinds of distances) can also be interpreted as a polyparacrystalline material. The single paracrystallites are built up by atoms with shorter distances. Neighbouring atoms, belonging to adjacent paracrystallites, give rise to the larger distances.

The next assumption is that all coordination statistics H_k projected on the respective mean direction of their correspondent distance vector $\mathbf{a}_k$ have the same shape. With respect to the isotropic character of a monatomic liquid this surely is a good approximation.

The analysis is carried out by means of a digital computer. By trial and error we choose different three-dimensional lattices, for instance a body-centered-cubic with the mean lattice parameter $\bar{a}$. At $r = \bar{a}\frac{1}{2}\sqrt{3}$ we meet the first eight atoms in the position $\pm\frac{1}{2}\pm\frac{1}{2}\pm\frac{1}{2}$ with the same coordination statistic $H(r)$, which is chosen arbitrarily. At $r = \bar{a}$ the next six distance-statistics are found. Following the concept of paracrystal they are given by $\widehat{HH}$. At $r = \bar{a}\sqrt{2}$ we find twelve atoms in the positions $[\pm 1; \pm 1; 0]$ with a distribution function $\widehat{HH}$. For, following the concept of paracrystals, two coordination vectors of the kind $(\frac{1}{2}\frac{1}{2}\frac{1}{2})$ are necessary to reach them. At $r = \bar{a}\frac{1}{2}\sqrt{11}$ in the position $\pm(\frac{3}{2}\frac{1}{2}\frac{1}{2})$ the next twenty-four atoms with a distribution function $\widehat{H\widehat{HH}}$ can be found and so on. Taking into account that correlations between adjacent atoms are not considered in the theory of paracrystals, but are more or less negligible for larger distances, we now use different lattice types, different shapes of H, different coordination numbers K and distances $\bar{a}$ until we finally obtain a folding polynom Eq. (10), which best fits the experimental function Eq. (20). for distances $r > 5$ Å. The differences observed between the experimental first distance statistics and the chosen coordination statistic H give direct information of next neighbour-correlations.

A secondary condition exists between K, $\bar{a}$ and the lattice type, to give the well known macroscopic density ρ_0 of the liquid. This restricts the variability of $\bar{a}$, and K for a certain lattice type.

Going on this line we have synthetisized many experimental radial density distribution functions, published by several authors on liquid Au, Ag, Pb, Mg, Na, K, Rb, Hg, Ar, Ne near the melting point.[20] In all cases we came to the following interesting conclusion:

The experimental radial density above about 5 Å can be synthetisized by a convolution polynom, if the following conditions are simultaneously fulfilled:

(1) The lattice must be hexagonal-close-packed. All other lattice types must be discarded. Even the face-centered-cubic lattice, which is quite similar to the hexagonal (ABCABC sequences instead of ABAB sequences) does not fit the experimental results, whatever K, $\bar{a}$ and the shape of H may be. Stacking faults at this

moment cannot be excluded. But they must be so small that the ABAB-sequences occur most frequently.

(2) The lattice must have a paracrystalline nature. All attempts to fit the experimental data by lattices which contain only conventional thermal distortions failed. But it could not be excluded that, besides distortions of the second kind a certain amount of distortions of the first kind (for details see[1,2]) exists. If $H_T(x)$ is the distribution function of the distance x of the centre of an atom from its mean position produced by thermal oscillations then all the humps in the convolution polynom $z(x)$ (cf. Eq. (10)) must be replaced by

$$H_p = \overbrace{H_T \widehat{H}_T \widehat{H} \widehat{H} \ldots \widehat{H}}^{(p+1) \text{ times}} \tag{21}$$

We could explain the experimental results by pure paracrystalline distortions as well as by smaller paracrystalline distortions in connection with distortions of the first kind. But it is impossible that the standard deviation Δr of H_1 is much higher than that of the Debye theory[12]

$$\Delta^2 r_D = \frac{144}{A\theta}\left[\frac{1}{4} + \frac{T}{\theta}\phi\left(\frac{\theta}{T}\right)\right] [\text{Å}^2] \tag{22}$$

(A atomic weight, T temperature (°K), θ characteristic temperature (°K), ϕ Debye function.)

Recent results of Averbach[15] for lead 2°C below the melting point can be analysed by our method too and prove that paracrystalline distortions exist.

(3) The paracrystalline coordination statistic $H_1(r)$ always had to consist of a symmetric part with a weight of about 80% of the whole statistic and of a tail with a weight of about 20%, whose centre lies at distances about 0.8 Å larger than that of the symmetric part. If generally α is the quotient of the weight of this tail and the whole coordination statistic, it means, that the averaged number of atoms, lying in a certain direction with smaller distances, is given by

$$\bar{N} = \frac{1}{\alpha}$$

Thus the relative weight of the tail gives information about the mean size of the paracrystals. In all cases we found sizes between 20 and 40 Å. Samples with temperatures much higher than the melting point showed smaller paracrystallites.

(4) For all molten metals the coordination number K was larger than that of a hexagonal lattice. Values of 13 to 14 (instead of 12) were observed. This agrees fairly well with the "mystic number" 14 of Bernal,[14] although our explanation is quite different from Bernal's: we explained this number by the existence of the above mentioned grain boundaries with 0.8 Å larger distances: Here each atom may have a larger number of more or less well defined "first neighbours".

With respect to the above mentioned correlations between first neighbours we get the following results comparing the experimental first peak (F.P.) with the symmetric part (S.P.) of the synthetic coordination statistic:

(5) The centre of F.P. lies always at about 0.1–0.2 Å smaller distances r than that of S.P. (cf. Table 1). Hence in the paracrystalline microlattices small groups of atoms build up entities with smaller inner-distortions. Such subgroups were observed by Honjo[13] in cubic crystals below the melting point too.

(6) Honjo's observations find another proof in the fact that the centre of (F.P.) even lies at 0.1 to 0.2 Å smaller distances than that calculated from the lattice constant of the crystal just below the melting point. Therefore, this lattice constant corresponds to the position of the centre of the whole coordination statistic H_1, since it is averaged over all lattice distances. Hence (F.P.) in the liquid gives information of next neighbour distortions, which are smaller than the distortions averaged over all distances in the solid crystal.

(7) As can be seen from Table 1 the Δr values of (F.P.) are nearly the same as of (T.D.), the thermal oscillations calculated by Eq. (22). The small entities of atoms within a paracrystal have practically only thermal, but no paracrystalline distortions.

(8) The centre of the whole asymmetric first distance statistic H_1 lies at about 0.1 to 0.2 Å larger distances than that calculated from a crystal. That is due to the fact that at the melting point H_1

TABLE 1 Mean Distance r (Å), Standard Deviation Δr(Å) and Coordination Number K of the Next Neighbour Statistics in Lead near and above the Melting Point

Temperature:	325° C			329° C			350° C			550° C		
References:	[15]			[15]			[16]			[17]		
	r	Δr	K	r	Δr	K	r	Δr	K	r	Δr	K
F.P.	3.48	0.29	12.1	3.39	0.30	12.6	3.38	0.28	11.7	3.40	0.35	9.5
H_1	3.56	0.34	11.9	3.69	0.51	13.1	3.69	0.42	13.2	3.63	0.58	12.3
S.P.	3.55	0.32	11.4	3.53	0.38	10.0	3.54	0.39	11.0	3.44	0.48	8.5
T.E.	—	0.27	—	—	0.31	—	—	?	—	—	?	—
T.D.	—	0.31	—	—	0.31	—	—	0.31	—	—	0.36	—
A.T.	3.77	0.1	0.5	4.44	0.4	3.1	4.16	0.4	2.2	4.21	0.3	3.8
P.S.		> 50 Å			22 Å			40 Å			12 Å	
g [%]		4.1			6.3			7.5			12.6	

F.P. = first experimental peak
S.P. = the symmetric part of H
T.E. = standard deviation of the distortions of the first kind (cf. Fig. 12)
A.T. = asymmetric part of H
g = g-value of the pure paracrystalline distorted first distance statistic H in [%]
H_1 = the total paracrystalline and thermal distorted coordination statistic = $\widehat{H}\widehat{H_T}\widehat{H_T}$
T.D. = thermal oscillations, calculated after Debye's Eq. (22)
P.S. = particle size of the microparacrystallites (Å)
? = the question marks indicate the values, which up to this moment are not yet calculated or measured

gets an asymmetric tail (A.T.) with a 0.8 Å larger mean distance. But the symmetric part (S.P.) of H_1 has, within the errors of experiment, about the same position as in the solid state. This means that the single paracrystallites in the liquid do not differ so much from the solid state.

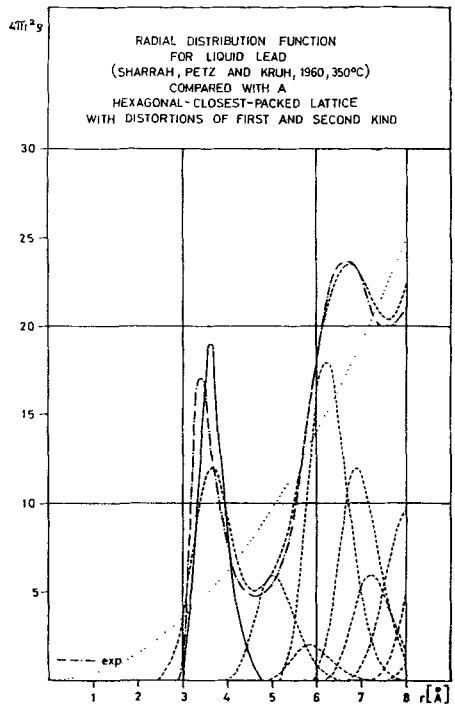

Figure 9. Radial distribution function for liquid lead measured by Sharrah *et al.* (1960) at 350° C compared with a hexagonal-close-packed lattice,[16] with distortions of the first and second kind.

Recent results of Averbach[15] 2° C below and above the melting point of lead can be analysed in the same way by convolution polynoms. Moreover, here one can analyse both distortions of the first and second kind. The standard deviation of the distortions of the first kind calculated from these experiments (T.E.) agrees well with that calculated from Debye's equation Eq. (22) (cf.

Table 1). The paracrystalline distortions Δr_p can be calculated from the values of Table 1 by

$$\Delta r_p = \sqrt{(\Delta^2 r_{(S.P.)} - \Delta^2 r_{(T.D.)})} \tag{23}$$

or from the slope of the σ^{-2} values against r in Averbach's paper and give rise to the g-values (cf. Eq. 15) in Table 1.

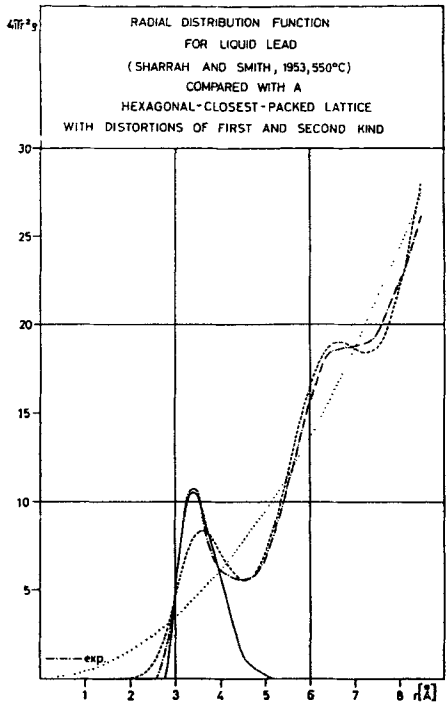

Figure 10. Radial distribution function for liquid lead measured by Sharrah *et al.* (1953) at 550° C [17] compared with a hexagonal-close-packed lattice with distortions of the first and second kind.

(9) Some important conclusions can be made: paracrystalline distortions exist not only above but also below the melting point. They increase with increasing temperature, mostly near the melting point.

(10) The discontinuity of density at the melting point is produced by the asymmetric tail (A.T.) of the coordination statistic H_1. At

the melting point small crystalline areas of 20–40 Å diameter remain nearly unchanged, but in between them grain boundaries arise with about 0.8 Å larger distances between neighbouring atoms. These larger distances seem to consume most of the melting

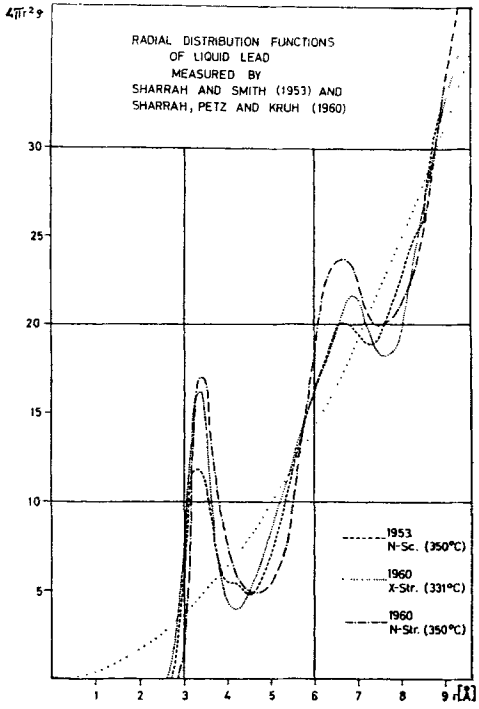

Figure 11. Comparison of the radial distribution functions of liquid lead measured by X-ray- and neutron-scattering (after Sharrah *et al.*, 1953 and 1960).

heat. In Fig. 9 the coordination statistic H of lead at 350° C calculated from radial distribution functions measured by Sharrah *et al.*[16] and all higher statistics $\widehat{HH}\ldots$ are reproduced. Their sum fits well with the experimental radial density distribution for $r > 5$ Å. The differences at smaller distances are caused by the small entities within single paracrystals, mentioned above. Figure 10 gives the

analysis of lead at 550° C.[17] Now the humps are so broadened, that the hexagonal-close as well as the cubic-close packing and the body-centred-cubic lattice may be introduced into the convolution polynom to give a good fit to the experimental curve. For g-values of about 12% and more all three lattice types give almost the same density distribution $\rho(r)$.

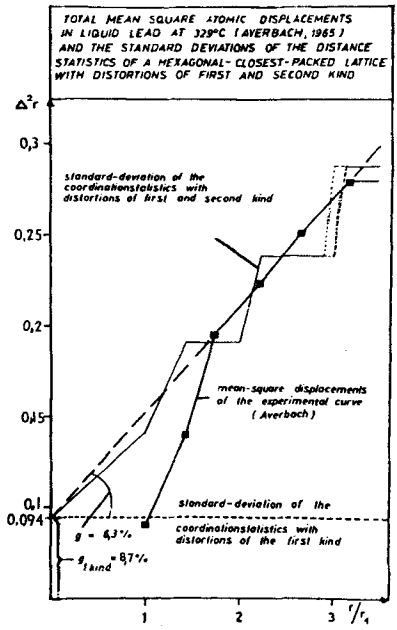

Figure 12. Total mean-square atomic displacement in liquid lead at 329° C (Averbach *et al.*, 1965) and the standard deviation of the distance statistics of a hexagonal-close-packed lattice with distortions of the first and second kind.

Figure 12 shows the $\Delta^2 r$-values of the single peaks of lead 2° C above the melting point calculated from the experiment by Averbach[15] compared with an adapted convolution polynom. Since at this temperature several humps of the nearest distances do not overlap, one can separate H from H_T (cf. Eq. (21)).

In Fig. 11 neutron and X-ray results of the same liquid lead,

published by Sharrah[16, 17] are compared. As long as the experimental techniques differ so much in their results, it is not useful to introduce further refinements into the theoretical calculations.

4. Metallic Alloys

Paracrystalline distortions can occur if in a regular crystal some of the atoms are statistically replaced by atoms with a larger diameter. We then have to deal with a "solid solution" or an

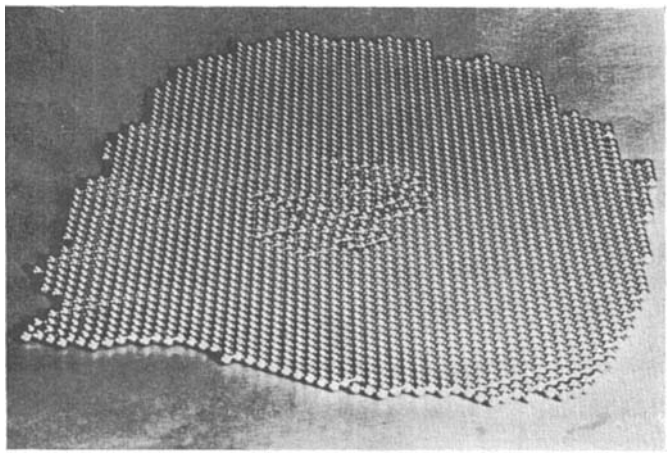

Figure 13. Two-dimensional steel ball model of a paracrystalline region.

"ideal mixed crystal" or a "Substitutions-Misch-Kristall". Figure 13 gives an idea of such a paracrystal: In a two-dimensional lattice of steel balls of 4 mm diameter some of them, in the central region, are replaced by steel balls with 4.5 mm diameter. The lattice planes are now curved, the distance between adjacent lattice planes changes statistically. If q is the amount of smaller atoms with diameter a, p that of the larger atoms with diameter $c=(a+\Delta)$, then the coordination statistic in a one-dimensional case is given by

$$H(x) = qP(x-a)+pP(x-c);\ p+q = 1 \qquad (24)$$

The mean distance $\bar{x}$ and the standard deviation Δx are given by

$$\bar{x} = \int_{\infty} xH(x)\,dx = qa + pc = a + p\Delta = c - q\Delta \tag{25}$$

$$\Delta x^2 = \int x^2 H(x+\bar{x})\,dx$$

$$= \int x^2(qP(x+p\Delta) + pP(x-q\Delta)\,dx = qp^2\Delta^2 + pq^2\Delta^2 = pq\Delta^2 \tag{26}$$

hence

$$g = \frac{\Delta x}{\bar{x}} = \frac{\Delta}{a+p\Delta}\sqrt{(p[1-p])} \tag{27}$$

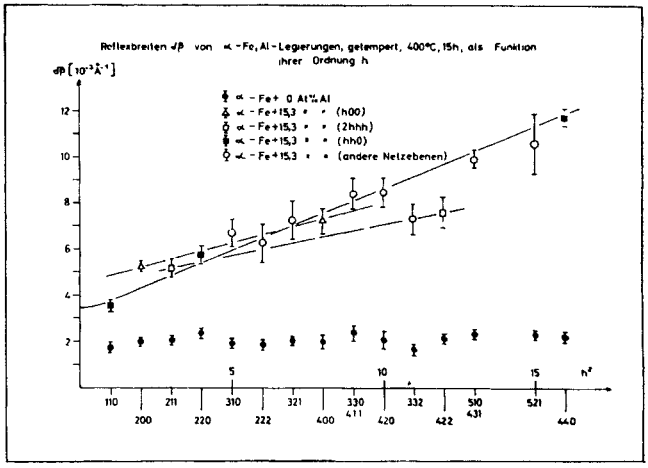

Figure 14. $\delta\beta$-h^2-diagram of the integral widths for different reflection groups from α-Fe-Al-alloys with 0 and 15.3 atom per cent Al, annealed 15 hr at 400° C.

In the three-dimensional case the g_{ik} values, defined by Eq. (15) are smaller than Eq. (27), since the atoms are aligned along curved rows. In crystals, moreover, the g_{ik}-values become smaller since the atoms do not behave like rigid balls, but have a certain amount of plasticity. Nevertheless, Eq. (25) is, too, a good approximation, an upper limit of the paracrystalline distortions to be expected for given Δ, a and p-values.

In the case of α-Fe, where p atom percent are replaced by Al, we know that $\Delta/a = 0.058$.

Figure 14 gives a $\delta\beta$ against h^2 plot of a series of Bragg-reflections,

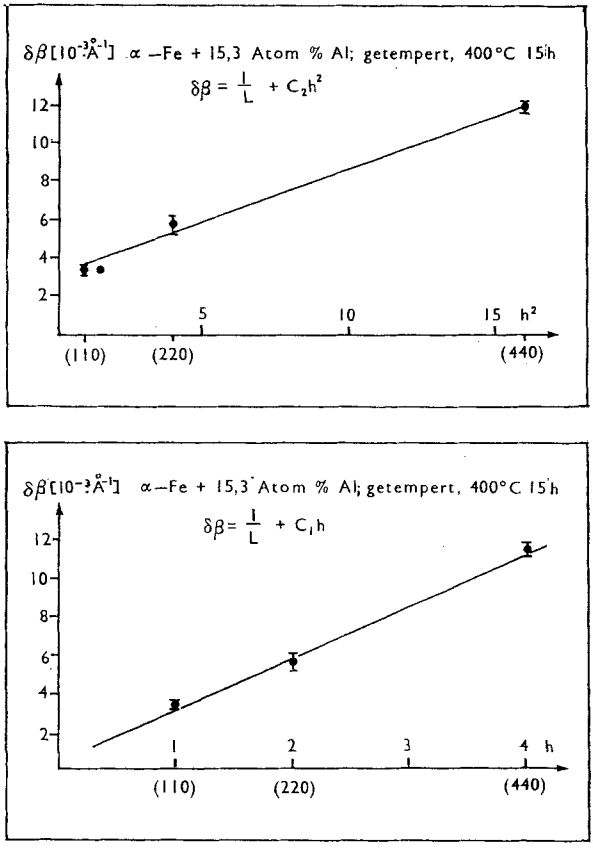

Figure 15. $\delta\beta$-h^2- and $\delta\beta$-h-diagram of the integral width for the reflections 110, 220 and 440 from α-Fe-Al alloy with 15.3 atom per cent Al, annealed 15 hr at 400° C.

for $p = 0$ and $p = 0.15$. To remove the microstrains, which give rise to line broadening, $\delta\beta$, proportional to h (see Fig. 4b), the samples were annealed 15 hr at 400° C before measurement. We see that for $p = 0$ all reflections have the same $\delta\beta$ within the error of the

experiments. Hence, in this case microstrains are absent. For $p = 0.15$ distortions remain.

Contrary to Fig. 4a, the $\delta\beta$-values as a function of h^2 do not lie exactly on a straight line (Fig. 15), since a certain amount of new microstrains arose during the annealing, since Al-atoms migrate at this temperature, and because their vapour pressure is relatively

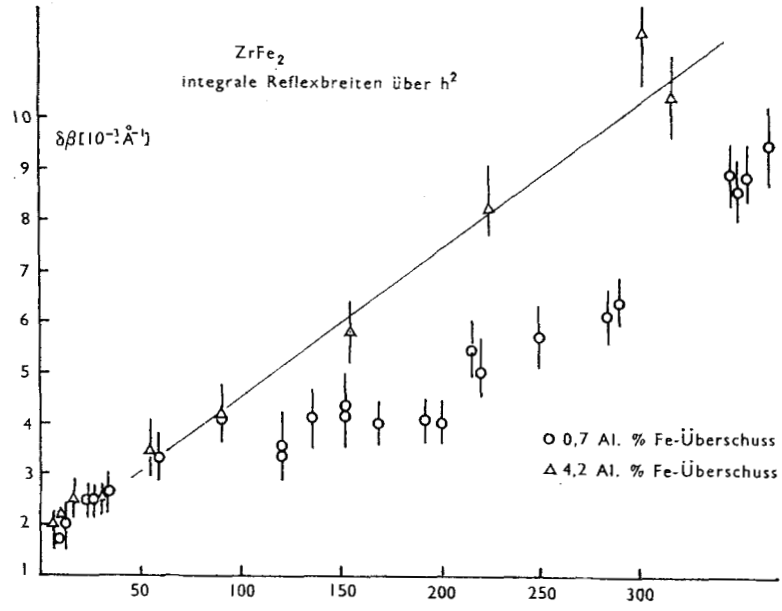

Figure 16. $\delta\beta$-h^2-diagram for reflections from $ZrFe_2$, with an excess of 0.7 and 4.2 atom per cent Fe.

high. Thus, the outer regions of single mosaic crystals have a lower amount p of Al-atoms and according to Eq. (25) the lattice parameter on the surface of these mosaic crystals becomes smaller. This gives rise to a $\delta\beta$ proportional to h trend. In Fig. 15 the $\delta\beta$-values of these (110)-reflections are plotted as h and h^2. The experimental curve lies between these two cases.

Nevertheless, a paracrystalline $\delta\beta$-h^2 linear relation remains to a certain degree. From the slope of this line one obtains for $p = 0.15$,

$$g = 1.05\%$$

The upper limit of Eq. (27) gives $g = 2.08\%$. The difference between the two values is a measure of the deformability of the non-rigid atoms. From Fig. 14 one can see that the g-values are different for different lattice planes (see Table 2). This gives interesting information about the coordination statistics, which in the case of the body centred α-Fe lie at $(\frac{1}{2}\frac{1}{2}\frac{1}{2})$, $(-\frac{1}{2}\frac{1}{2}\frac{1}{2})$, $(\frac{1}{2}-\frac{1}{2}\frac{1}{2})$ and $(\frac{1}{2}\frac{1}{2}-\frac{1}{2})$. In Fig. 16 a $\delta\beta$ against h^2 plot of Fe_2Zr is reproduced. This alloy is a "Laves-phase". The Zr-atoms built up a lattice of the diamond type. In each of the interstices of this lattice four Fe-atoms are arranged in a

TABLE 2 Paracrystalline Distortions in Mixed Crystals

Lattice	Foreign atoms	p (%)	Lattice plane	g (%)	g_{rigid}
α Fe	—	0	All	0	0
α Fe	Al	15	(110)	1.05	—
			(200)	0.7	2.08
			(211)	0.63	
Fe_2Zr	Fe	0.7	(222)	0.3	?
		4.2	(222)	0.66	
Carbonyl Fe	—	0			
	AlOOH(?)	3	(110)	1.0	
			(200)	1.15	?
			(211)	0.73	

tetrahedron. Even if there is no excess of Fe-atoms, g-values could be observed (Table 2). This means that statistically some of the Fe-atoms occupy interstitial positions and hence give rise to paracrystalline distortions. Here, contrary to Fig. 15, the $\delta\beta$-values of all reflections lie on one line, which can be explained by the irregular (statistical isotropic) interstitial position of some Fe-atoms.

Though all the paracrystalline lattices described in this section have nothing to do with a liquid crystal, it must be emphasized that these distortions again destroy the long-range order of a real crystal and give rise to special mechanical and physico-chemical properties of these materials, which cannot be understood from the concept of a conventional real crystal.

5. Reduced Spinels

We also found paracrystalline distortions in reduced spinels of Fe_2O_3, Fe_3O_4 with statistically inserted Al_2O_3. Such reduced spinels play an important role as catalysts. Most of the papers published on this subject assume that, after reduction in H_2 at 400° C, the Al-atoms migrate to the boundary of the microcrystallites. Our careful analysis of the line widths $\delta\beta$ against h^2 proved that at least a certain amount of Al after reduction must stay within the α-Fe-lattice.

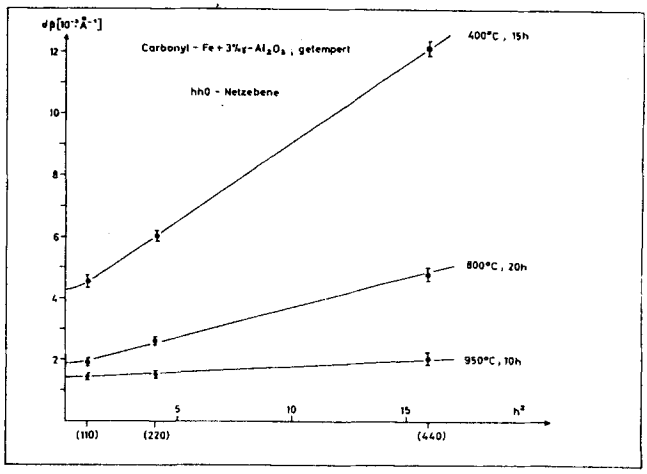

Figure 17. $\delta\beta$-h^2-diagram of the reflections 110, 220 and 440 from Carbonyl-Fe + 3% γ-Al_2O_3, annealed in various ways.

In Fig. 17 the $\delta\beta$-h^2 plot of the hh0 reflections clearly proves this fact. From its slope for $p = 3$ atomic per cent Al we found a g-value of

$$g = 1.02\%$$

Contrary to the above mentioned Fe-Al-alloys the g-value in these reduced spinels does not drop markedly after annealing at 800° C (Fig. 17). Hence the Al-atoms cannot be built into the lattice as metallic atoms but perhaps as AlOOH compounds. This is quite probable since, contrary to Fe-Al-alloys, here the lattice parameter

is not increased with increasing amount of Al. From Eq. (25) (Vegards rule) we see that here the foreign atoms cannot change the volume of the lattice. Taking into account that AlOOH crystals are known in nature as Böhmit and Diaspor, which have nearly the same c-axis as the lattice parameter of α-Fe, we have here the interesting example of compounds built into the α-Fe lattice which

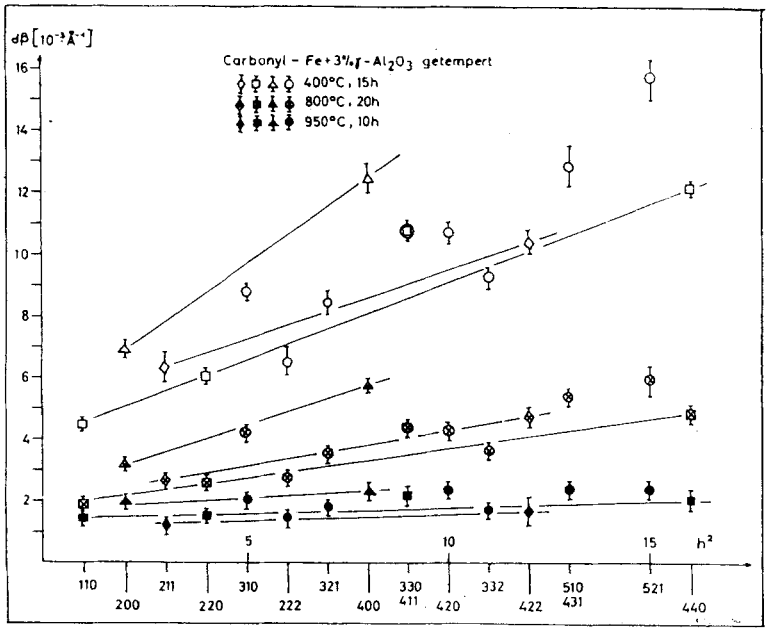

Figure 18. δ-βh^2-diagram of all measured reflections from Carbonyl-Fe + 3% γ-Al_2O_3, annealed in various ways.

do not change the lattice constant, but as a consequence of their different shape nevertheless produce paracrystalline distortions.

Here again in different directions we find other g-values (Fig. 18). Contrary to Fe-Al-alloys now the g-value of the (200) lattice planes is the largest one, which gives information about the shape and position of the foreign subgroups of Al, O and H-atoms in the α-Fe-lattice.

Acknowledgments

We thank Dipl.-Phys. A. Schönfeld and cand. phys. F. Vogel, who carefully measured the line widths of metallic alloys by means of an AEG-double cylinder precision camera using a fine-focus X-ray tube. Grateful acknowledgment is due to the Deutsche Forschungsgeneinschaft for supporting our investigations. Finally we thank Prof. Dr. R. Brill, Berlin, and Prof. Dr. G. Schulze, Dresden, for the supply of samples.

REFERENCES

1. Hosemann, R. and Bagchi, S. N., *Direct Analysis of Diffraction by Matter* (North-Holland Publ. Comp., Amsterdam, 1962).
2. Guinier, A., *X-Ray Diffraction in Crystals, Imperfect Crystals, and Amorphous Bodies* (W. H. Freeman and Comp., San Francisco and London, 1963).
3. See reference 1, above, p. 286.
4. Bonart, R., Hosemann, R., and McCullough, R. L., *Polymer*, **4**, 199 (1963).
5. See reference 1, above, p. 325.
6. Hosemann, R., Wilke, W., and Balta Calleja, F. J., *Acta Cryst.* **21**, 118 (1966).
7. Friedel, J., *Dislocations* (Pergamon Press, Oxford, 1964).
8. Hosemann, R. and Wilke, W., *Z. Faserforsch. u. Textiltechn.* **15**, 521 (1964).
9. Bonart, R., *Z. f. Krist.* **109**, 296 (1957).
10. Holland, V. F., *J. Appl. Phys.* **35**, 3235 (1964).
11. Hosemann, R., and Lemm, K., edit. J. A. Prins, *Phys. Non-Cryst. Solids* (North Holland Publ. Comp., 85, 1965).
12. See reference 1, above, p. 276.
13. Honjo, G., Kodera, S., and Kitamura, N., *J. Phys. Soc. Jap.* **19**, 351, (1964.)
14. Bernal, J. D., *Nature* **185**, 65 (1960).
15. Kaplow, R., Strong, S. L., and Averbach, B. L., *Phys. Rev.* **138**, A 1336 (1965).
16. Sharrah, P. C., Petz, J., and Kruh, R. F., *J. Chem. Phys.* **32**, 241 (1960).
17. Sharrah, P. C. and Smith, G. P., *J. Chem. Phys.* **21**, 228 (1953).
18. Hosemann, R., Bialas, D., Schönfeld, A., Wilke, W., and Weick, D., *Advances in Materials*, (Pergamon Press, pp. 81–93, 1966).
19. Eckstein, B., *Habilitationsschr.* (T. H. Aachen, 1965).
20. Lemm, K., *Dissertation* (F. U. Berlin 1966).